RESEARCH ARTICLE

Synthesis, Characterization, Thermal and Biological Study of New Organic Compound with Some Metal Complexes

Nawras A. Ouj[1], Enass J. Waheed[2]*

[1,2]*Department of Chemistry, College of Education for Pure Sciences, Ibn -Al-Haitham, University of Baghdad, Adhamiyah, Baghdad, Iraq.*

Received: 18th March, 2021; Revised: 09th April, 2021; Accepted: 28th May, 2021; Available Online: 25th June, 2021

ABSTRACT

A new set of metal complexes by the general formula $[M(P)_2(H_2O)_2]Cl_2$ has been prepared through the interaction of the new Ligand [N1, N4-bis(4-methoxyphenyl)succinamide] (P) derived from succinyl chloride with p-anisidine with the transition metal ions [Cu(II), Mn(II), Cd(II), Co(II) and Ni(II)]. Compounds diagnosed by TGA, ^{1}H, ^{13}CNMR and Mass spectra (for (P)), Fourier-transform infrared and Electronic spectrum, Magnetic measurement, molar conduct, (%M, %C, %H, %N). These measurements indicate that (P) is associated with the metal ion in a bi-dentate fashion by nitrogen atoms (the amide group), and the octahedral composition of these complexes is suggested. *Staphylococcus Aureus* (+) and *Escherichia Coli* (–) were studied for the antibacterial action of the compounds towards two types of bacteria. Using SKOV3-type ovarian cancer cell lines and comparing them to the normal cell line, the cell viability and cytotoxicity assay were performed on the Cu (II) complex by anticancer activity.

Keyword: Anticancerious, Biological activity, Succinyl chloride.

International Journal of Drug Delivery Technology (2021); DOI: 10.25258/ijddt.11.2.30

How to cite this article: Ouj NA, Waheed EJ. Synthesis, Characterization, Thermal and Biological Study of New Organic Compound with Some Metal Complexes. International Journal of Drug Delivery Technology. 2021;11(2):401-408.

Source of support: Nil.

Conflict of interest: None

INTRODUCTION

Aniline is one of the most organic compounds (toxic). Aniline is involved in the synthesis of many organic compounds via azo dyes, corrosion inhibitors, pesticides, antioxidants, rubber, antiseptics, pharmaceuticals, and fuel additives, due to the wastewater structure for pharmaceutical production dyestuffs, and its high toxicity due to their aniline content harm aquatic ecosystems.[1,2] Aniline derivatives contribute to the manufacture of paints, pharmaceuticals, rubber, dyes, herbicides, pigments, and precursors to polyurethane. Although aniline compounds produced in some pharmaceutical factories are organic in nature, they are very complex in composition, causing high resistance to biological degradation.[3] The p-Anisidine is a well-known ligand containing a methoxy group that gives an electron, and this makes the donor nitrogen atom rich in electrons.[4,5] Substitution of the methoxy group on the ring (2, 3, or 4 methoxyaniline) determines the ability of the ligand to donate an electron and a potential steric obstruction. It is also used to detect unsaturated aldehydes in food quality testing and prepare 1-methoxy-4-trans-Styryl-benzene by reaction with phenylbenzene and biochemical research organic synthesis.[6-8] The aim of the current study to define the structure and geometry of (P) and its complexes to ions Mn(ii), Co(ii), Ni(ii), Cu(ii), and Cd(ii).

EXPERIMENTAL SECTION

Materials and Methods

From commercial sources, we obtained all chemical and analytical reagents and were used without further purification. From (the United States of America, Sigma - Aldrich, Merck, and India), various chemicals, metal salts, and solvents used in this research were purchased. Infrared spectroscopy was measured using the device (Shimadzu FTIR affinity-1s) and Potassium bromide (KBr) disc within the range 400–4000 cm^{-1}). Through the use of an electrothermal melting point device (SMP10 Stuart), the melting point of the compounds prepared in an open tube was determined. Using (Shimadzu UV-1800) visible, ultraviolet spectrophotometer with a concentration of 3^{-10} M samples in dimethyl sulfoxide (DMSO) solvent at room temperature and a quartz cell length of 1.0 cm, the electron spectra of the prepared compounds were measured. Using the device (Bruker 300 MHz NMR spectrometer), the chemical displacements were recorded in (NMR spectra ^{1}H and ^{13}C) in (DMSO-d6 with TMS). Using a device (Shimadzu (AA 680)), %M in complexes is determined. Using a device (Philips pw-Digital conductivity meter), the molar conductivity of the prepared compounds was

*Author for Correspondence: enasshassanali@gmail.com

measured with a concentration of (10^{-3}M) in (DMSO) and at room temperature. Using a device (magnetic sensitivity balance (Sherwood Scientific)), (μeff BM) of complexes were measured at room temperature. Using a device (Euro EA 300), (%C, %H, %N) was determined for the prepared compounds. A STA PT-1000 Linseis at the temperature range of 0-700^{0}C and used argon gas, thermal gravity analysis (TGA) was performed.

The Organic Compound

Synthesis of Ligand (P)[9]

A solution of 0.999 g (6.45 mmol) of Succinyl chloride in acetone (10 mL) was slowly added to a solution of p-Anisidine (1.588 g, 12.9 mmol) in acetone (10 mL) over 1-hour. The mixture was stirred for 12 hours at $^-5$°C and then for 2 hours at laboratory temperature. The precipitate formed was filtered and then washed with solvent (diethyl ether) and then recrystallized in ethanol and left to dry at laboratory temperature. m.p. 168-170°C (yield 86%) (Scheme 1), (Figure 1).

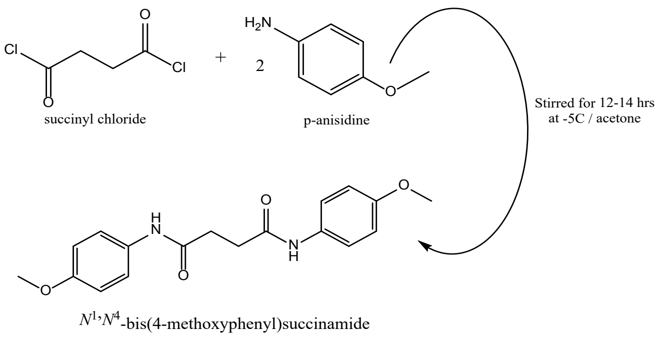

Scheme 1: Preparation course of the (P)

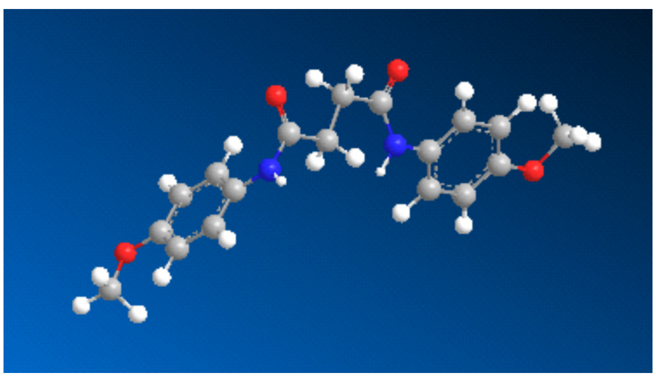

Figure 1: 3D –Structure of the (P)

The Inorganic Compounds

Synthesis of $[M(P)_2(H_2O)_2]Cl_2$: To (P) solution (0.66 gm, 2 mmol) in (10 mL) EtOH, the metal chloride solution ($MnCl_2.4H_2O$, $CoCl_2.6H_2O$, $NiCl_2.6H_2O$, $CuCl_2.6H_2O$ and $CdCl_2.H_2O$) (0.24–0.17 gm, 1 mmol) in (10 mL) EtOH was added. Under reflux, the reaction mixture was heated for 4 hours. The precipitate formed was filtered and then washed with solvents (H_2O and diethyl ether) and in a laboratory atmosphere, leave dry (Figure 2).

RESULTS AND DISCUSSION

Thermal stability and the nature of the colored solid are the most important characteristics of the prepared metal complexes—insolvents (DMSO) and (DMF), soluble. The theoretical and practical data of (AA) measurements for all prepared complexes were approximated in Table 1.

Mass Spectral

The mass spectral data fragmentation of (P) [N1,N4-bis(4-methoxyphenyl) succin amide], Figure (3) showed (M+) at

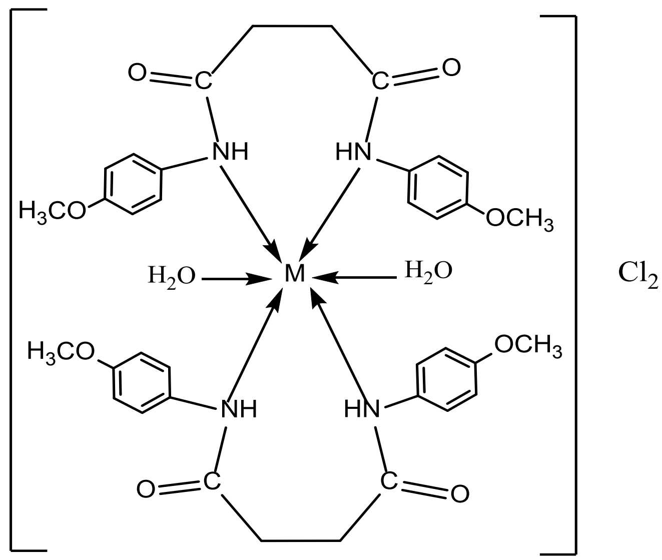

Figure 2: Suggested structure for (P) complexes

Table 1: Different physical properties of the prepared compounds

Com.	*(Formula wt.)*	*m.p(°C) or d*	*Color*	*Metal% Calculated (Actual)*	*Conducts Ohm^{-1}cm^{2}mol^{-1} in solvent (DMSO)*
Ligand (P)	$C_{18}H_{20}N_2O_4$ 328	168-170	grey	-----	1.67
Mn - P	$C_{36}H_{44}Cl_2MnN_4O_{10}$ 818.60	125-127	Brown	6.71 (6.70)	74.1
Co - P	$C_{36}H_{44}Cl_2CoN_4O_{10}$ 822.60	121-124	Green	7.16 (7.17)	75.2
Ni - P	$C_{36}H_{44}Cl_2NiN_4O_{10}$ 822.36	115-117	Green	7.14 (7.12)	72
Cu - P	$C_{36}H_{44}Cl_2CuN_4O_{10}$ 827.21	111-114	Brown	7.68 (7.66)	70.1
Cd - P	$C_{36}H_{44}Cl_2CdN_4O_{10}$ 876.08	118-120	grey	12.83 (12.84)	83

(m/z+=328) Due to (the original molecular weight of P) (328) , [$C_{18}H_{20}N_2O_4$]. Additional peaks are displayed in Table 2.[10,11]

NMR Spectra

^{1}H-NMR Spectra of (P)

In order to confirm the structure of the ligand (P), ^{1}HNMR of the synthesized ligand was recorded. Figure (4) display the ^{1}HNMR of the ligand, the peak at (δ 2.66 ppm) corresponds to four aliphatic protons of succinyl group, and peaks at (δ 6.90–δ7.57 ppm) correspond to the all aromatic protons of the ligand. the peak at (δ 10.13 ppm) represents the proton of (–CO-NH-) moiety, whereas the peak at (δ 9.93 ppm) reverts to the proton of (NH) group specifically .the peak at (δ 2.78–δ3.83ppm) correspond to the protons of (CH_3) and (OCH_3) group .finally the peaks at (δ 2.39 – δ 2.57 ppm) correspond to residual protons in DMSO-d^6 and moisture present in DMSO-d^6.[12-13] The results are summarized in Table 3.

^{13}C-NMR Spectra of (P)

The ^{13}C-NMR spectrum, for ligand (P) portrays is shown in Figure 5; the spectrum exhibits signals at chemical shift (δ=174.06 ppm), which assign to ($C_{1,1^-}$) for (CO-NH) amide group. The chemical shifts at (δ =155.41-159.05 ppm), assigning to ($C_{2,2^-}$) for the aromatic ring. The chemical shift at (δ =133.05, 124.76, 124.83 and 114.25 – 114.53ppm) attributed to the aromatic ring ($C_{3,3^-}$) , ($C_{4,4^-}$) and ($C_{5,5^-}$) respectively. Chemical shift-related carbons ($C_{6,6^-}$) for (OCH_3) in p-anisidine and ($C_{7,7^-}$) for (CH_2) in succinyl group appeared at (δ = 55.61 -55.93) and (31.71ppm) respectively. Finally chemical shift at (δ = 39.17–40.84 ppm) which assign to DMSO.[14,15] The results are summarized in Table 4.

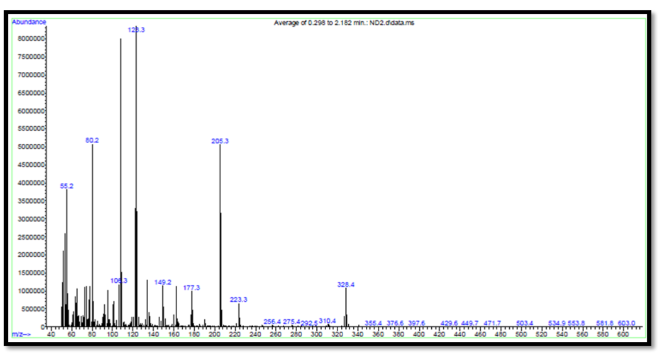

Figure 3: EI mass spectrum of P.

Table 2: The fragmentation pattern of (P)

Fragment	*Mass/charge (m/z)*	*Relative abundance*
[$C_{18}H_{20}N_2O_4$]	328	13.65 %
[$C_{11}H_{15}N_2O_3$]$^{+\cdot}$	223	7.5 %
[$C_{11}H_{11}NO_3$]$^{+\cdot}$	205	62.5 %
[$C_{10}H_{11}NO_2$]$^{+\cdot}$	177	12.5 %
[$C_8H_7NO_2$]$^{+\cdot}$	149	13.75 %
[C_7H_9NO]$^{+\cdot}$	123	100 %
[C_7H_6O]$^{+\cdot}$	106	90 %
[C_6H_8]$^{+\cdot}$	80	62.5 %
[C_4H_7]$^{+\cdot}$	55	47.5 %

FTIR Spectra

Ligand (P)

The band at 3309 cm^{-1} the spectrum of the (P) determined to the υ(NH), while another absorption band showed at 1647 cm^{-1} could be interpreted as υ(C=O amide), in addition

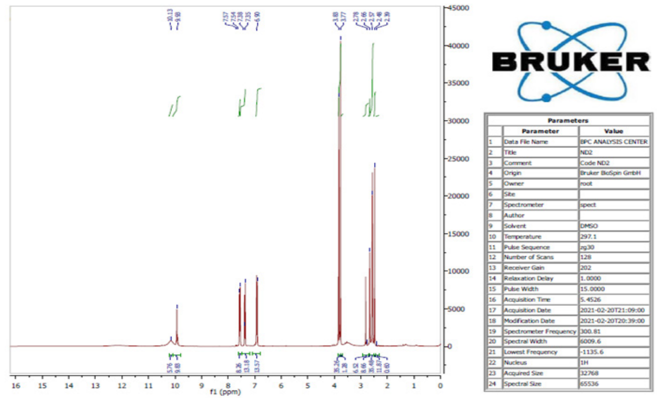

Figure 4: ^{1}H-NMR spectra of (P)

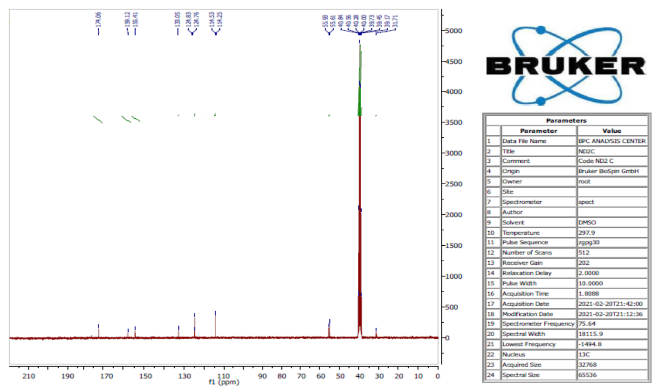

Figure 5: ^{13}C-NMR spectra of (P)

Table 3: Chemical shifts in (^{1}H-NMR) spectra of (P)

Com.	*Functional groups*	*δ (ppm)*
Ligand (P)	Aliphatic proton (4H)	2.66
	2-aromaticprotons(8H)	6.90–7.57
	2-CO-NH-moiety(2H)	10.13
	2NH group (2H)	9.93
	2CH_3 group (6H)	2.78
	2OCH_3 group (6H)	3.83
	DMSO-d6 solvent	2.39–2.57

Table 4: Chemical shifts in (^{13}C-NMR) spectra of (P)

Com.	*Functional groups*	*δ (ppm)*
Ligand (P)	$C_{1,1^-}$ for (CO-NH) amide group	174.06
	$C_{2,2^-}$ for aromatic ring	155.41–159.05
	$C_{3,3^-}$ for aromatic ring	133.05
	$C_{4,4^-}$ for aromatic ring	124.76–124.83
	$C_{5,5^-}$ for aromatic ring	114.25–114.53
	$C_{6,6^-}$ for (OCH_3) in p-anisidine	55.61–55.93
	$C_{7,7^-}$ for (CH_2) in succinyl group	31.71
	DMSO	39.17–40.84

Table 5: FTIR data of (P) (cm^{-1}) and their complexes.

Comp.	*υ(C-H) Arom.*	*υ(C-H) Aliph.*	*υ(N─H)*	*υ(C=O) amide*	*OCH_3))δ*	*υ(M-N)*	*δ(M-O) of water*
Ligand-p	3008	2935	3309	1647	2835	-	-
Mn-p	3103	2962	3407	1647	2837	466	925
Co-p	3089	2933	3427	1650	2837	470	925
Ni-p	3072	2939	3425	1649	2835	472	923
Cu-p	3010	2935	3417	1650	2837	472	925
Cd-p	3014	2912	3425	1650	2838	472	925

Table 6: Electronic transfers in the spectra of the prepared compounds

Com.	λ_{nm}	*υ (cm^{-1})*	ε_{max} *(moler^{-1}. cm^{-1})*	*Transition*	*Shape geometry*
Ligand (P)	290	34482	3643	$\pi \rightarrow \pi^*$	-
Mn-p	300 888 994	33333 11261 10060	3976 11.5 55.0	Intra Ligand $^6A_{1g} \rightarrow {}^4T_{2g(G)}$ $^6A_{1g} \rightarrow {}^4T_{1g(G)}$	Octahedral
Co-p	310 390 862 888 990	32258 25641 11600 11261 10101	3859 3950 14.0 16.0 60.0	Intra Ligand C.T $^4T_{1g\,(f)} \rightarrow {}^4T_{1g\,(P)}$ $^4T_{1g\,(f)} \rightarrow {}^4A_{2g\,(P)}$ $^4T_{1g\,(f)} \rightarrow {}^4T_{2\,g}$	Octahedral
Ni-p	284 498 918 992	35211 20080 10893 10080	3479 894 9.0 12.0	Intra Ligand $^3A_{2g} \rightarrow {}^3T_{1g\,(p)}$ $^3A_{2g} \rightarrow {}^3T_{2g\,(f)}$ $^3A_{2g} \rightarrow {}^3T_{2g\,(f)}$	Octahedral
Cu-p	300 408 862 916 962	33333 24598 11600 10917 10395	3820 3857 553 524 512	Intra Ligand C.T $^5B_{1g} \rightarrow E_g$ $^5B_{1g} \rightarrow {}^5B_{2g}$ $^5B_{1g} \rightarrow {}^5A_{1g}$	Distorted Octahedral
Cd-p	320 400	31250 25000	3807 475	Intra Ligand C.T	Octahedral

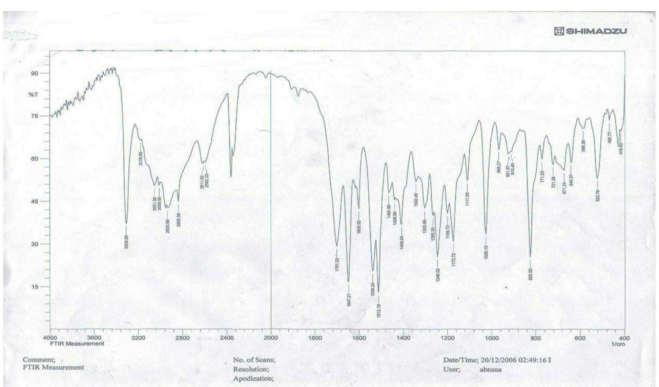

Figure 6: FTIR spectrum of (P).

to absorption bands at (2935) due to υ(C-H aliphatic), (3008) cm^{-1} due to υ(C-H aromatic) and (2835) cm^{-1} which determined to $\delta(OCH_3)$,[16] Figure 6.

Complexes of Ligand (P)

These spectra showed a marked various between bands belonging to the stretching vibration of υ(NH, amide group) in the range between (3427–3407) cm^{-1} shifted to higher

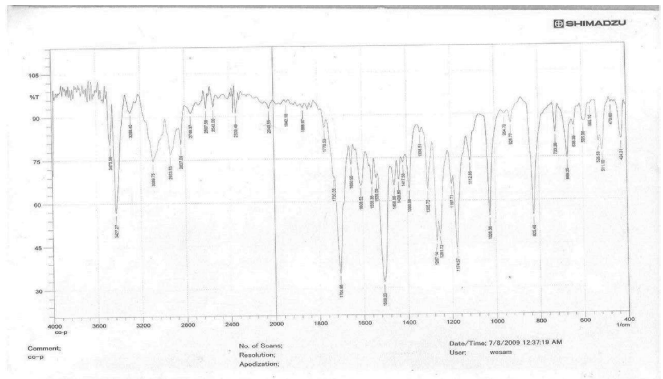

Figure 7: FTIR spectrum of [Co-P] complex.

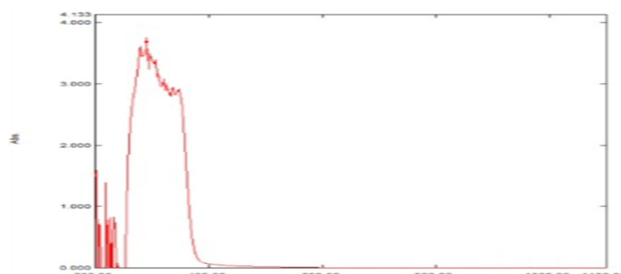

Figure 8: Electronic spectrum of the P.

frequencies by (118–98) cm^{-1} proposing the probability of the co-ordination of (P) by the nitrogen atom at the amide group.[17,18] The υ(C=O, amide) in ligand was not correlated with the central ion and was confirmed by no changes in the frequencies of this group that were set at (1650–1647) cm^{-1} in the complexes spectrum of the ligand complexes.[19,20] New bands υ(M-O, water group) and υ(M-N, amide group) appeared in the range of (923–925) cm^{-1} and (466–472) cm^{-1}, respectively, indicating the formation of the metal complexes.[21,22] In Table 5, FTIR data is displayed. In Figure 7, the spectra of the (P) and its complexes were presented.

Electronic Spectra

Ligand (P)

The electronic spectrum of (P) in DMSO solution is including in Figure 8. The spectrum display absorption peak at (290 nm =34482 cm^{-1} ; ε_{max}= 3643 molar^{-1} cm^{-1} which assigned to ($\pi \rightarrow \pi^*$).[23] In Table 6, data are recorded.

Complexes of Ligand (P)

The electronic spectrum of the Mn (ii) - complex display peaks in the (d-d) region at 888 nm, which due to $^6A_1g \rightarrow {}^4T_{2}g_{(G)}$

transition and 994 nm assigned to $^6A_1g \rightarrow {}^4T_1g_{(G)}$. Another peak in the 300 nm which assigned to intra ligand, these all indicating octahedral geometry about Mn ion.[24]

The Co (ii)-complex shows peaks at 310 nm attributed to intra ligand and 390 nm due to CT. Another peak at 862 nm due to $^4T_{1g\,(F)} \rightarrow {}^4T_{1g\,(P)}$ transition, 888nm due to $^4T_{1g\,(F)} \rightarrow {}^4A_{2g}$, and 990 due to $^4T_{1g\,(F)} \rightarrow {}^4T_{2g}$. These electronic transitions revealed by the cobalt complex refer to the octahedral geometry of the aforementioned complex.[25]

The electronic spectrum of the Ni^{II} - complex display in the (d-d) region (peaks) at 498 nm assigned to $^3A_{2g} \rightarrow {}^3T_{1g\,(P)}$ transition, 918 nm due to $^3A_{2g} \rightarrow {}^3T_{1g(F)}$, and 992 due to $^3A_{2g} \rightarrow {}^3T_{2g\,(F)}$. Another peek at 284 nm due to intra ligand indicates

The electronic spectrum of the Cu (ii)- complex display in the (d-d) region (peaks) at 862 nm attributed to (d-d) type $^5B_{1g} \rightarrow E_g$, and 916 nm due to $^5B_{1g} \rightarrow B_{2g}$ and 962 nm due to type $^5B_{1g} \rightarrow {}^5A_{1g}$. Another peek at 300 nm and 408 nm due to intra ligand and CT these all confirming distorted octahedral geometry about Cu ion.[27]

The electronic spectra of the Cd-complexes exhibited peaks at (320, 400) nm, which were due to (intra-ligand) and CT, respectively, these all indicating octahedral geometry about Cd ion.[28] In Table 6, UV data of compounds was displayed.

Magnetic Moments and Conductivity Measurements

In Table 5, the (μeff) values of Mn(ii), Co(ii), Ni(ii), and Cu(ii) complexes are display. These complexes exhibit μeff (5.164, 4.277, 3.259 and 1.893) B.M respectively, these normal values are consistent with high spin octahedral complexes.[29] The electrolytes nature (1:2); M^{+2}= Mn(ii), Co(ii), Ni(ii), and Cu(ii) and Cd(ii) complexes of all metal complexes was confirmed by molecular conductivity measurements,[30] Table 1.

Cell Viability and Cytotoxicity Assays

Based on a tetrasolium salt - (4,5-dimethyl-thiazol-2-yl)-2,5-diphenyltetrazo-lium bromide (MTT), cytotoxicity was measured by colorimetric assay. On the protocol that Tim Mossman first described in 1983, the MTT test was adopted in anticancer activity.[31] The SKOV3 tumor cell lines were compared with the normal (WRL-68) cell line used in our current study. At concentrations ranging from 400-6.25 μg/mL of Cu (II), the SKOV3 cell line and the normal cell line (WRL-68) have been shown.

The toxic effect was estimated by extracting the percentage of inhibition compared to control (100% growth). The Fresney method has been used to develop the ovarian cancer cell line SKOV3. By way of analyzing a single method of variance ANOVA (Duncan), the data are statistically analyzed, which is performed to test whether or not the variance in the group is significant. Using SPSS version 20 and flooding it with Graph Pad Prism Version 6, data were expressed as mean, standard error, and statistical significance implemented. The relationship between the biological activity of linear cancer cells in ovarian SKOV3 and normal cells (WRL-68) is illustrated in Figures 10 and 11. By applying different concentrations of the metal complex Cu (II) to cell lines, this test was performed to measure the vitality of cells and the rate of inhibition of them. Using log (inhibitor) against response curve, data analysis performed in μg/mL, and log values for μg/mL were plotted on the Prism 6 graph pad.

To clarify the effect of the copper complex on the types of cancerous and normal cells, it was observed that the lowest rate of inhibition of cell growth was at 6.25 μg/mL and the highest rate of inhibition of (400 μg/mL) for the concentration of ovarian cells SKOV3 and normal cells (WRL-68).

According to the type of cell line, the rates of Cu (II) inhibition will vary. Between (84.57–35.58)% for the SKOV3 ovarian cancer cell line and (95.33–69.28)% for the normal (WRL-68) cell line, determined the number of live cells remaining after interaction with the copper complex. The highest percentage of inhibition of normal cells is the most (WRL-68) 69.28%, while the highest percentage of inhibition

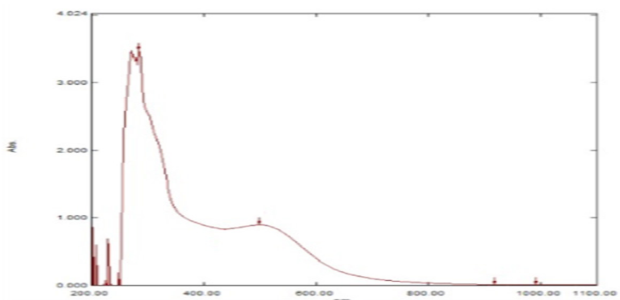

Figure 9: Electronic spectrum of [Ni-P] complex.

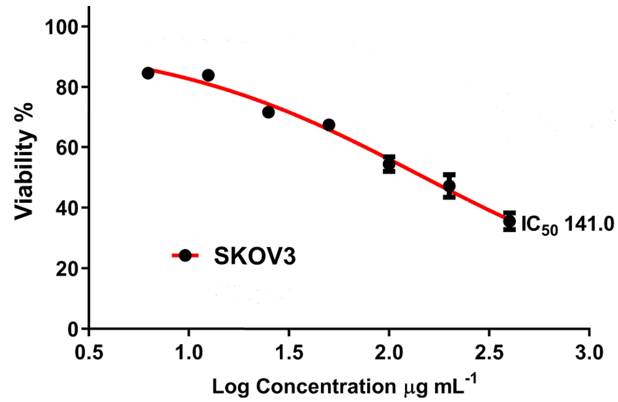

Figure 10: Cytotoxicity effect of [Cu-P] on SKOV3 cells after (24 hours) incubation at 37ºC.

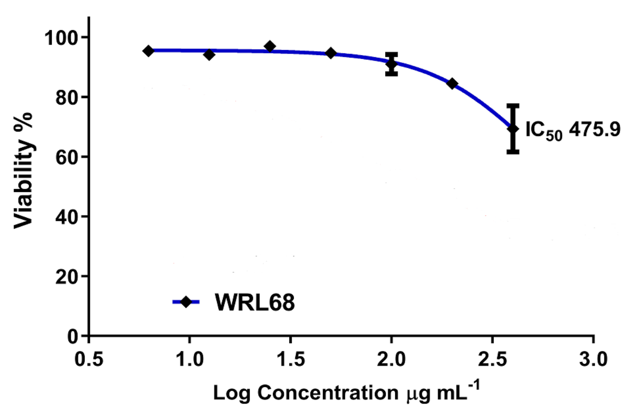

Figure 11: Cytotoxicity effect of [Cu-P] on (WRL68) cells after (24 hours) incubation at (37ºC).

Table 7: For the same concentration using MTT assay at 37°C (24-hrs), the effect of [Cu-P] on ovarian cancer cell line (SKOV3) was demonstrated and compared with normal cell line (WRL68)

Inhibition concentration Ic_{50}	*Concentrations used mg/mL Percentage of ovarian cell rate Average ± standard error))*					
	25	*50*	*100*	*200*	*400*	*Cellular lines*
141.0	71.64 ± 1.33	67.44 ± 1.80	54.48 ± 2.41	47.21 ± 3.73	35.58 ± 2.77	Cytogenetic cell lines of ovarian
475.9	96.95 ± 1.14	94.64 ± 1.51	90.97 ± 3.30	84.46 ± 0.85	69.28 ± 7.72	natural cells line (WRL68)

Table 8: Results obtained from the biological activity of the prepared compounds.

No.	*Compounds*	*Escherichia coli*	*Staphylococcus aureus*
1	Ligand (P)	16	19
2	Mn-P	15	14
3	Co-P	11	15
4	Ni-P	20	17
5	Cu-P	15	15
6	Cd-P	16	22

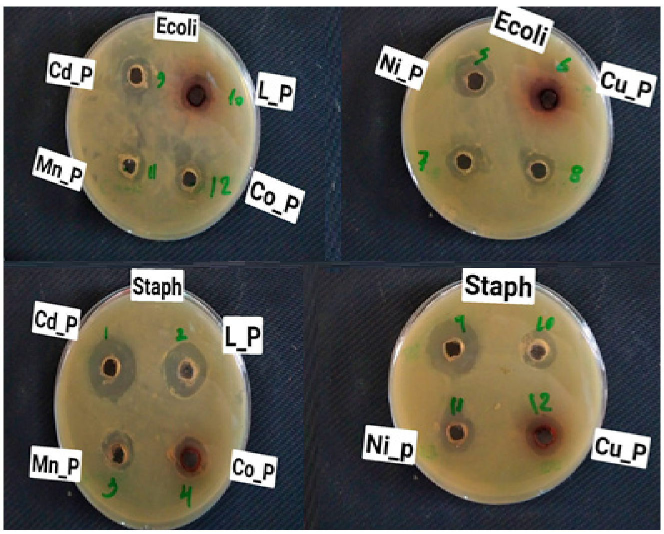

Figure 12: Figures of the biological activity of the prepared compounds

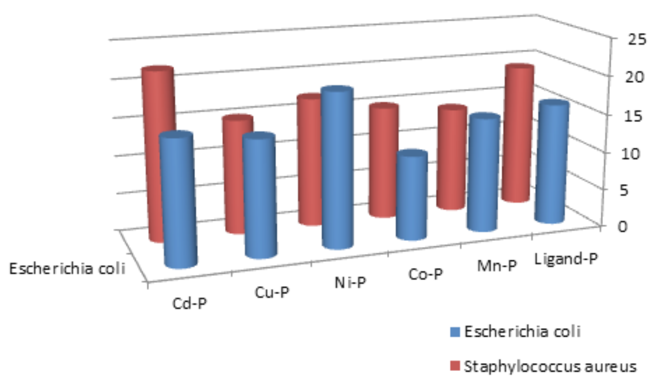

Figure 13: Graph of the results of the bioactivity of the prepared compounds.

of Cu (II) compound for the line of ovarian cancer cells in SKOV3 is 35.58%, this is what was observed. One of the important results obtained through tests of SKOV3 cancer cell lines is (IC50) (inhibitor Concentration Fifty). This concentration, in turn, kills approximately half of the cells, Table 7.

Table 9: Temperature values for analysis along with corresponding weight loss values.

		TGA			
			Found (calculate)		
Com.	*Stage*	*Thermo Gravimetry range (°C)*	*Loss of Mass (mg)*	*Total mass lose (mg)*	*Fragmenta-tion*
Ligand	1	170-295	1.06 (1.045)	3.767	2H, 2N ,2O
(P)	2	296-325	0.54 (0.56)	(3.757)	3C
	3	326-405	1.278 (1.266)		6C, 8H
	4	406-597	0.887 (0.886)		4C , 8H

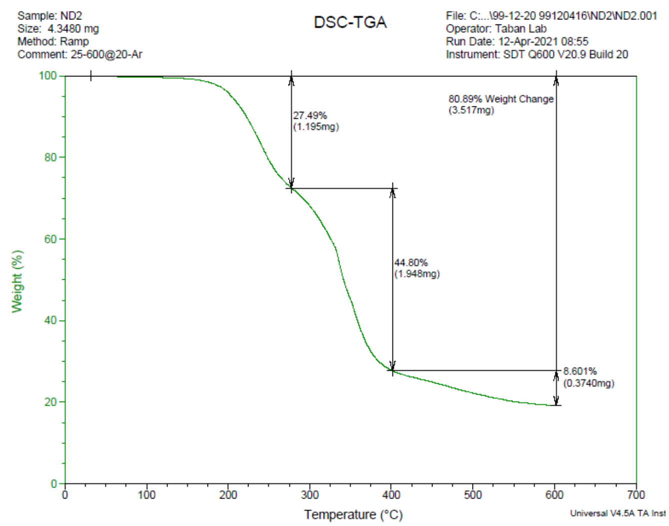

Figure 14: Thermal study of (P)

The half inhibitor is equal to (141.0 μg/mL) in the case of the interaction of Cu complex with the SKOV3 ovarian cancer cell line, where we note that the concentration of the inhibitor (IC50) falls within the concentrations from which (IC50) is taken for the normal cell line (WRL-68) it is (475.9 μg/mL).[32,33]

Anti-bacterial Activity Studies

Staphylococcus aureus (G^+) and *Escherichia coli* (G^-) were used as test micro-organisms. The medium surface was inoculated and covered for the purpose of performing the assay on test organisms. Before applying disks, allow the agar surface to dry from 3 to 5 minutes. The tablets were dipped in a chemical beaker using sterile forceps and placed in the medium previously. To grow, the bacteria plates were incubated at 37°C for 48 hours. The complexes show different activity in limiting bacterial proliferation compared to ligand (P) in concentrations prepared.[34-35] The results obtained are recorded in Table 8, Figures 12, and 13.

Thermal Analysis

The ligand (P) was prepared and subjected to thermal analysis using a STAPT-1000 Linseis company1 Germany. In an atmosphere of argon gas, this measurement was done within the temperature range (0–700)°C and heating rate 10°C/min.[36,37] Where it was recorded all results are derived from the TG curves for the ligand (P) examined in Table 9, Figure 14.

CONCLUSION

This search showed the prepared and identification of (P) and its Mn (ii), Co (ii), Ni (ii), Cu (ii), Cd (ii) compounds. The octahedral geometry of the prepared complexes was suggested depending on the results (^{1}HNMR, Mass spectra, and ^{13}CNMR of (P) only), magnetic measurement, and molar conductivity of the compounds. The (P) acts as bidentate and coordinates by the N atoms in (NH-C=O) group. The thermal decomposition steps of the different parts of the prepared ligand (P) were determined by studying TGA. The (P) and its complexes were examined for their antibacterial activities against two types of bacteria. By using SKOV3-type ovarian cancer cell lines and comparing them to the normal cell line, the cell viability and cytotoxicity assay was performed on the Cu (II) complex by anticancer activity as drugs to treat some cancerous diseases that affect humans.

REFERENCES

1. Nelson DL, Cox MM. Amino acid oxidation and the production of urea. Lehninger principles of biochemistry. 2000;3:623-658.
2. Zhao C, An J, Zhou L, Fei Q, Wang F, Tan J, Shi B, Wang R, Guo Z, Zhu WH. Transforming the recognition site of 4-hydroxyaniline into 4-methoxyaniline grafted onto a BODIPY core switches the selective detection of peroxynitrite to hypochlorous acid. Chemical Communications. 2016;52(10):2075-2078.
3. Anand S, Kalainathan S, Amrutha TV, Senthil K, Yamada M. Investigation on the growth, structural, optical, thermal and third-order nonlinear optical (NLO) properties of 2, 3-dimethyl-N-[(E)-2, 4, 5-trimethoxybenzylidene] aniline (DTA) organic single crystal. Journal of Materials Science: Materials in Electronics. 2021 Apr;32(8):11059-11071.
4. Siva V, Bahadur SA, Shameem A, Murugan A, Athimoolam S, Suresh M. Synthesis, supramolecular architecture, thermal and optical behavior of 4-methoxyanilinium perchlorate: A promising third-order NLO material for optical limiting device applications. Optical Materials. 2019 Oct 1;96:109290.
5. Enass JW. Synthesis, Spectral and Thermal Characterization of Ni(II), Cu (II) and Zn(II) Complexes with New Ligand Towards Potential Biological Application. Biochemical and Cellular Archives, 2020; 20(1):2483-2494.
6. Al-Amery MH. Synthesis and Charac terization of New Complexes of (N-4-Methoxy Phenyl) Amino Phenyl Acetonitrile Ligand with Some Divalent Transition Metal Ions. Al-Nahrain Journal of Science. 2012 Sep 1;15(3):55-61.
7. Pandya JH, Jadeja RN, Ganatra KJ. Spectral characterization and biological evaluation of Schiff bases and their mixed ligand metal complexes derived from 4, 6-diacetylresorcinol. Journal of Saudi Chemical Society. 2014 Jul 1;18(3):190-199.
8. Shaygan S, Pasdar H, Foroughifar N, Davallo M, Motiee F. Cobalt (II) complexes with Schiff base ligands derived from terephthalaldehyde and ortho-substituted anilines: synthesis, characterization and antibacterial activity. Applied Sciences. 2018 Mar;8(3):385.
9. Karaböcek N, Karaböcek S, Mazlum H, DEĞİRMENCİOĞLU İ, Serbest K. Synthesis and characterization of Cu (II) complexes of two ligands derived from malonyl dichloride. Turkish Journal of Chemistry. 2004 Mar 16;28(1):87-94.
10. Buchcic A, Zawisza A, Leśniak S, Adamczyk J, Pieczonka AM, Rachwalski M. Enantioselective Mannich reaction promoted by chiral phosphinoyl-aziridines. Catalysts. 2019 Oct;9(10):837.
11. Sarhan BM, Kadhim NJ, Wheed EJ. Stability constant of some Metal Ion Complexes of (6-(2Amino-2-(4-hydroxy phenyl)-acetamido)-3, 3--dimethyl-7oxo-4-thia-1-aza-bicyclo [3, 2, 0] heptanes-2carboxylicacid (Amoxicillin). Ibn AL-Haitham Journal For Pure and Applied Science. 2017 Apr 24;26(3):245-253.
12. Waheed EJ, Ahmed AA. Synthesis, Characterization, Thermal Study, Biological Activity and Corrosion Inhibition of New Ligand Derived from Butanedioyl Dichloride and Some Selective Transition Metal Complexes. Journal of Global Pharma Technology, 2019;11(2): 379-391.
13. Sarhan BM, Lateef SM, Waheed EJ. Synthesis and Characterization of Some Metal Complexes of [N-(1, 5-dimethyl-3-oxo-2-phenyl-2, 3-dihydro-1H-pyrazol4-ylcarbamothioyl) acetamide]. Ibn AL-Haitham Journal For Pure and Applied Science. 2017 Mar 16;28(2):102-115.
14. Salah BA, Kandil AT, Abd El-Nasser MG. Synthesis, molecular docking and computational studies of novel hydrazone complexes. Journal of Radiation Research and Applied Sciences. 2019 Jan 2;12(1):413-422.
15. Cordeiro GM, Hottes E, Esteves-Souza A, Guedes GP, de Sant'Anna CM, Herbst MH. A Novel ZnII Complex Bearing Two Monodentate (4-Methoxyphenyl)[(1E, 2E)-3-phenylprop-2-en-1-ilidene] Schiff Bases: Crystal Structure and DFT Study. Journal of Chemistry. 2019 Feb 11;2019:1-6.
16. Dahi MA, Jarad AJ. Synthesis, characterization and biological evaluation of thiazolyl azo ligand complexes with some metal ions. InJournal of Physics: Conference Series 2020 Nov 1 (Vol. 1664, No. 1, p. 012090). IOP Publishing.
17. Mas-Roselló J, Smejkal T, Cramer N. Iridium-catalyzed acid-assisted asymmetric hydrogenation of oximes to hydroxylamines. Science. 2020 Jun 5;368(6495):1098-1102.
18. Radja I, Djelad H, Morallon E, Benyoucef A. Characterization and electrochemical properties of conducting nanocomposites synthesized from p-anisidine and aniline with titanium carbide by chemical oxidative method. Synthetic Metals. 2015 Apr 1;202:25-32.
19. Kupko N, Meehan KL, Witkos FE, Hutcheson H, Monroe JC, Landee CP, Dickie DA, Turnbull MM, Xiao F. Cobalt halide complexes of 2-, 3-and 4-methoxyaniline: Syntheses, structures and magnetic behavior. Polyhedron. 2020 Sep 1;187:114680.
20. Petrović VP, Simijonović D, Milovanović VM, Petrović ZD. Acetophenone Mannich bases: study of ionic liquid catalysed synthesis and antioxidative potential of products. Royal Society open science. 2018 Nov 1;5(11):181232.
21. Lüthi E, Forero Cortés PA, Prescimone A, Constable EC, Housecroft CE. Schiff base ancillary ligands in bis (diimine) copper (I) dye-sensitized solar cells. International journal of molecular sciences. 2020 Jan;21(5):1735.
22. More PS, Mehta BH. 1H NMR, Diffused Reflectance, Thermal studies, ESR And Anti microbial Activities Of Schiff Base Derived From 5-Nitro Salicylaldehyde and p-Anisidine.

International Letters of Chemistry, Physics and Astronomy. 2015;48:14-26.

23. Sathiyanarayanan V, Prasath PV, Sekhar PC, Ravichandran K, Easwaramoorthy D, Mohammad F, Al-Lohedan HA, Oh WC, Sagadevan S. Docking and in vitro molecular biology studies of p-anisidine-appended 1-hydroxy-2-acetonapthanone Schiff base lanthanum (iii) complexes. RSC Advances. 2020;10(28):16457-16472.
24. Ashiq M, Danish M, Mumtaz MW, Rafique S, Hussain T. Physico-Chemical and Toxicological Properties of Para-Anisidine based Sulfonamides: Theoretical Approach and Experimental Justification. Journal of the Chemical Society of Pakistan. 2017 Feb 1;39(1):125-131.
25. Kholoud R. Synthesis, physicochemical characterization and cytotoxic activity of p-methoxyphenyl and p-fluorophenyl maleanilic acid and their corresponding Cr, Mo and W metal carbonyl novel Organometallic Chelates. Journal of Transition Metal Complexes. 2020 Feb 27;3:1-9.
26. Malik MA, Dar OA, Gull P, Wani MY, Hashmi AA. Heterocyclic Schiff base transition metal complexes in antimicrobial and anticancer chemotherapy. MedChemComm. 2018;9(3):409-436.
27. Sales ES, Schneider JM, Santos MJ, Bortoluzzi AJ, Cardoso DR, Santos WG, Merlo AA. Quinolines by three-component reaction: synthesis and photophysical studies. Journal of the Brazilian Chemical Society. 2015;26:562-571.
28. Hammami A, Rabti A, Raouafi N. A novel electrochemical and chromogenic guest-responsive anisidine-based chemosensor for transition metallic cations. Journal of Electroanalytical Chemistry. 2014 Oct 1;731:179-183.
29. Obaleye JA, Tella AC, Obiyenwa GK, Simon N, Olawale MD. Zinc (II) Complex of Meso-Tetraphenylporphyrin With 4-Methoxyaniline: Crystal Structure and Antimicrobial Activities of 4-Methoxyaniline-5, 10, 15, 20-Tetraphenyl-Porphyrinatozinc (II). Synthesis and Reactivity in Inorganic, Metal-Organic, and Nano-Metal Chemistry. 2016 Apr 2;46(4):589-95.
30. Bashir S, Teo YY, Ramesh S, Ramesh K, Rizwan M. Synthesis and characterization of pH-sensitive n-succinyl chitosan hydrogel and its properties for biomedical applications. Journal of the Chilean Chemical Society. 2019 Sep;64(3):4571-4574.
31. RamaDevi V, Radha V, VijayaKumar B, Ravikumar K, Vithal M. Synthesis and reactivity in inorganic, metal-organic, and nano-metal chemistry. 2014;44(7):1-8.
32. Waheed EJ, Farhan MA, Hameed GF. Synthesis and Characterization of new Manganese (II), Cobalt (II), Cadmium (II) and Mercury (II) Complexes with ligand [N-(3-acetylphenylcarbamothioyl)-2-chloroacetamide] and their Antibacterial Studies. InJournal of Physics: Conference Series 2019 Jul 1 (Vol. 1234, No. 1, p. 012096). IOP Publishing.
33. Liz-Andela NI, Benitez R, Martin-Franco J, Rojas G. Tunable polyesterification of xylitol: from linear to crosslinked structures. Polymer International. 2017 Apr;66(4):532-539.
34. Al-Khateeb ZT, Karam FF, Al-Adilee K. Synthesis and characterization of some metals complexes with new heterocyclic azo dye ligand 2-[2--(5-Nitro thiazolyl) azo]-4-methyl-5-nitro phenol and their biological activities. InJournal of Physics: Conference Series 2019 Sep 1 (Vol. 1294, No. 5, p. 052043). IOP Publishing.
35. Ahmad F, Alkahtani MD, Taj MB, Alnajeebi AM, Alzahrani SO, Babteen NA, Alelwani W, Bannunah AM, Noor S, Ayub R, Tirmizi SA. Synthesis of New Naphthyl Aceto Hydrazone-Based Metal Complexes: Micellar Interactions, DNA Binding, Antimicrobial, and Cancer Inhibition Studies. Molecules. 2021 Jan;26(4):1044-1090.
36. Molano MF, Lorett VP, Erben MF. Crystal structure, spectroscopic characterization and Hirshfeld surface analysis of aquadichlorido{N-[(pyridin-2-yl)methylidene]aniline}copper(II) Monohydrate. Acta Cryst. 2020;76(2):48-154.
37. Subashini G. Bhagavannarayana and K. Ramamurthi .Synthesis, growth, crystalline perfection of 4-bromo-40dimethylamino benzylideneaniline (BDMABA) and photons absorption of BDMABA crystal. Molecular and Biomolecular Spectroscopy. 2013;104:403–408.